Received: 5 November 2023 | Revised: 18 December 2023 | Accepted: 31 December 2023

DOI: 10.1002/mop.34013

RESEARCH ARTICLE

WILEY

Using generative model for intelligent design of dielectric resonator antennas

Mingdian Liu[1] | **Hui Zhang**[2] | **Jiming Song**[1] | **Meng Lu**[1,3]

[1]Department of Electrical and Computer Engineering, Iowa State University, Ames, Iowa, USA

[2]School of Information and Communication Engineering, Communication University of China, Beijing, China

[3]Department of Mechanical Engineering, Iowa State University, Ames, Iowa, USA

Correspondence
Mingdian Liu and Jiming Song, Department of Electrical and Computer Engineering, Iowa State University, Ames, IA 50011, USA.
Email: menglu@iastate.edu and jisong@iastate.edu

Funding information
National Science Foundation, Grant/Award Number: ECCS 16-53673

Abstract

In the advancing field of 5G technologies, particularly at the 60 GHz band, dielectric resonator antennas (DRAs) stand out for their low conduction loss and high radiation efficiency. However, the traditional design process for DRAs, predominantly reliant on intuitive reasoning and trial-and-error methods, is notably inefficient and resource-intensive. Addressing this critical challenge, our research introduces a pioneering approach: a generative adversarial network (GAN)-based model specifically tailored for automating DRA structure design. This novel model represents the first of its kind in the domain, marking a significant departure from conventional methods. Our GAN model uniquely integrates a simulator for DRA modeling and a generator for DRA structure design, streamlining the design process. To effectively train this model, we created a simulated data set comprising pattern–annotation pairs of geometric shapes and S_{11} parameters. This data set enabled the GAN to capture the intrinsic principles underlying DRA design. The practical impact of our model is profound; it significantly expedites the DRA design process, aligning it more closely with specific user requirements while conserving valuable time and resources. This breakthrough approach not only enhances the efficiency of DRA design but also sets a new standard in antenna technology development for future wireless communications.

KEYWORDS

deep learning, dielectric resonator antenna, generative model, inverse design

1 | INTRODUCTION

The advent of millimeter-wave (mmWave) 5G technology at 60 GHz has created a demand for antennas with high bandwidth, high gain, and temperature-independent performance, all while maintaining a small footprint.[1] Within this framework, dielectric resonator antennas (DRAs) emerge as a compelling substitute for traditional metal antennas.[2] DRAs offer a range of benefits including a lack of conduction losses and high radiation efficiency at high frequencies. Additionally, the use of dielectric materials with a high dielectric constant allows for antennas with a reduced footprint. Dielectric resonators can be designed in a variety of shapes to fit specific application requirements for better integration into antenna design. Meanwhile, DRAs can also show excellent

Mingdian Liu and Hui Zhang contributed equally to this study.

properties of impedance matching and mode matching.[3,4] Several DRA designs for 5G applications have been demonstrated in recent years.[5–10] However, the current design process relies heavily on prior knowledge of designers, and there are currently no established design rules for the V-band (60 GHz) frequency range.

Artificial intelligence breakthroughs offer a new avenue for automating antenna inverse design. Thanks to the availability of big data and increasing computational power, deep learning has shown enormous potential for rackling complex processing tasks. Multilayer perceptions, autoencoder, and generative adversarial networks (GANs), for instance, can capture the underlying pattern in complex data sets and leverage them to create new data sets that may not be intuitive to humans.[11–15] This paper demonstrates a GAN model for the inverse design of DRAs and explores its ability to generate customized antenna structures. It is worth noting that the antenna performance is usually determined by many factors and our work focuses on the design of the DRA geometry using the GAN model.

2 | DRA DESING AND MODELING

2.1 | mmWave DRNA design

The mmWave DRA structure, illustrated in Figure 1A, consists of a dielectric resonator mounted on a half-mode substrate-integrated waveguide (HMSIW).[16] The HMSIW, designed as a substrate-integrated waveguide, utilizes two metal plates surrounding a dielectric substrate containing metallic vias to guide and reflect electromagnetic signals. The tapered line serves as the transition between the HMSIW and microstrip line, while a transverse rectangular slot enables the excitation signal to feed the dielectric resonator from the HMSIW. The substrate is comprised of a dielectric material (Rogers 5880) low permittivity and loss tangent of 2.2 and 0.001 at 50 GHz, respectively. The DRA structures are made of a high dielectric constant material (Rogers TMM10i) with a permittivity of 10 and a loss tangent of 0.002. The DRA resonator shape largely determines the antenna's radiation characteristics. Our objective is to design and train a deep learning model capable of predicting a DRA's S_{11} without using a full-wave electromagnetic simulation while also generating new DRA geometries based on a desired S_{11} spectrum.

2.2 | Numerical simulation

Using the finite element method (FEM) by Ansys HFSS, we simulated the radiation characteristics of a group of DRAs with different dielectric resonators but sharing the same HMSIW substrate. As an example, Figure 1B,C showcase the simulation results for the DRA with a star-shaped resonator. The HMSIW had geometric parameters of $w_{ms} = 0.35$ mm, $l_{ms} = 10$ mm, $w_{tr} = 0.9$ mm, $l_{tr} = 1.4$ mm, $w = 2.2$ mm, $l = 8.9$ mm, $d = 0.4$ mm, $s = 0.5$ mm, and a dielectric thickness of 0.127 mm. The dielectric resonator, with the star shape (inset of Figure 1B) and a thickness of 0.5 mm, was simulated for its reflection coefficient in the frequency range of 45–65 GHz. The resulting S_{11} spectrum (Figure 1B) exhibited a bandwidth of 32.0% for $|S_{11}| < -10$ dB at the DRA resonance around 63.8 GHz. The 47.6 GHz resonance, which associated with the HMSIW slot, was also

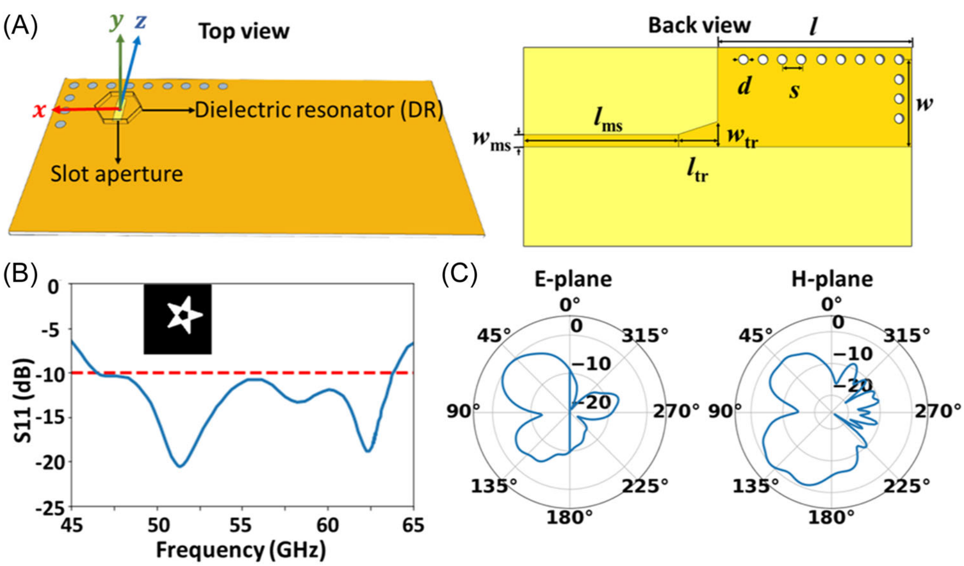

FIGURE 1 (A) Schematic diagram of a hexagon-shaped DR antenna (DRA) on a half-mode substrate-integrated waveguide substrate (top and back view). (B) The finite element method simulation of S_{11} spectrum for the star-shaped DRA is shown in the inset. (C) Simulated patterns at 50 GHz along the E-plane (xy-plane) and H-plane (yz-plane), respectively.

observed. Furthermore, the radiation pattern of this DRA structure was simulated at 50 GHz and presented in Figure 1C, revealing a near omnidirectional pattern across most of the radiation angles.

3 | DESIGN AND TRAINING OF NEURAL NETWORK

3.1 | Design of the GAN model

The conventional GAN model can generate synthetic patterns that resemble ground truth data distribution, aided by a noise input.[11] However, modified GAN models such as conditional GAN (cGAN), auxiliary classifier GAN, and InfoGAN have been developed to incorporate supplementary information into the input data, enabling the production of data corresponding to specific target labels.[17–19] To streamline the design and modeling of DRAs, we present a GAN model based on cGAN. The proposed GAN deep learning network is depicted in Figure 2A, consisting of generator, simulator, and critic networks. These networks are primarily designed based on the convolutional neural network (ConvNet), which is utilized to extract spatial features from the two-dimensional (2D) DRA resonator geometries.[20] Each neural network block, consisting of ConvNet, batch normalization (BN) layer, and residual neural network (ResNet),[21,22] as depicted in Figure 2B, is repurposed within the GAN deep learning network. The BN facilitates output data renormalization and maintains convergence, while the ResNet helps alleviate gradient explosion and vanishing commonly encountered during ConvNet-based neural network training. The simulator (Figure 2C) takes geometric shapes as input and predicts the S_{11} parameters (S') of the corresponding DRA pattern. This module has been trained to serve as a substitute for full-wave simulation. The critic classifier, shown in Figure 2C, is employed to distinguish between generated geometric shapes and pre-existing ones. As depicted in Figure 2B, the generator, featuring a reverse architecture of the simulator, is trained in conjunction with the critic to penalize discrepancies between the actual S_{11} parameters (S) and the reconstructed S', as well as errors made by the critic classifier. By introducing noise (z), the GAN model can generate a diverse range of data randomly sampled from the distribution acquired during training. The source code can be accessed at the following link: https://github.com/mingdianliu/AntennaGAN.

3.2 | Generation of training data set

To create the learning data set, a group of DRA structures were simulated using the FEM. The cross-sections of these DRAs were generated by using a subset of a public data set of 2D geometric shapes.[23] The 2D patterns include nine groups of geometries: circles, heptagons, hexagons, nonagons, octagons, pentagons, squares, stars, and triangles, as shown in Figure 3A. We randomly selected the perimeter, center position, and rotation range of these geometries to generate a set of 5040 patterns. From each geometric category, we chose 560 patterns and pixelized them into 32×32 binary arrays, which represent the horizontal cross-section of the DRAs (Figure 3A). The resonators were formed on the HMSIW using the high dielectric constant material with a thickness of 0.127 mm. A MATLAB script

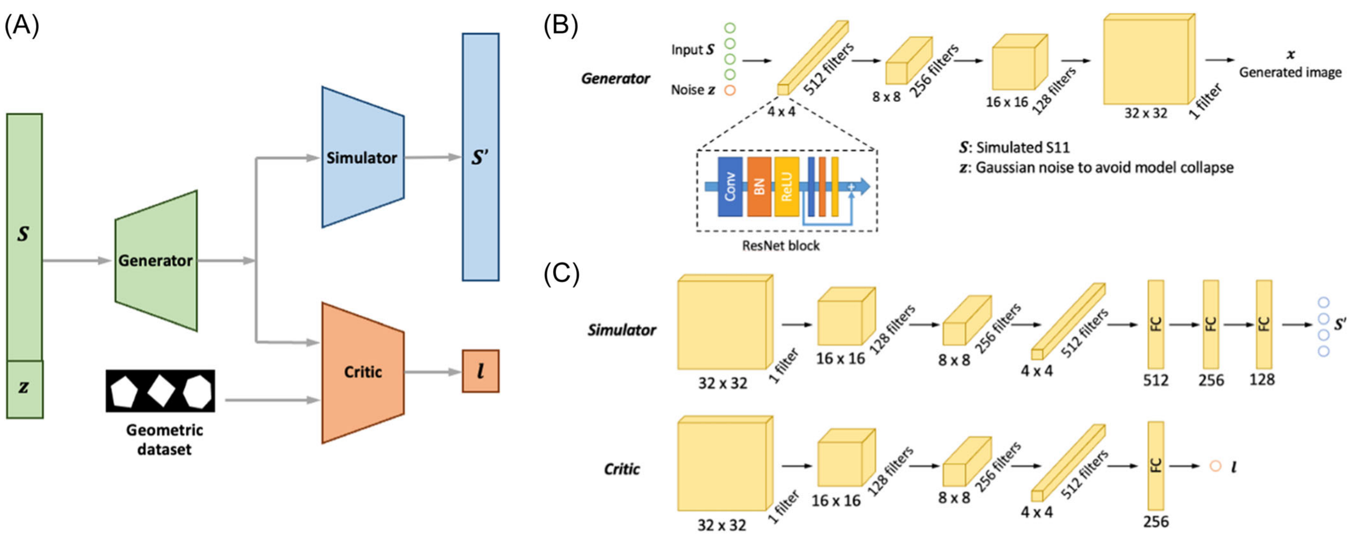

FIGURE 2 (A) Generative adversarial network model based on generator, simulator, and critic networks. The inputs of the generator network (B) include the training S_{11} data and Gaussian noise. The generator output, representing the calculated DRA pattern, is used as an input of the simulator and critic networks. (C) Simulator and critic networks consisting of the convolutional neural network, batch normalization, and residual neural network.

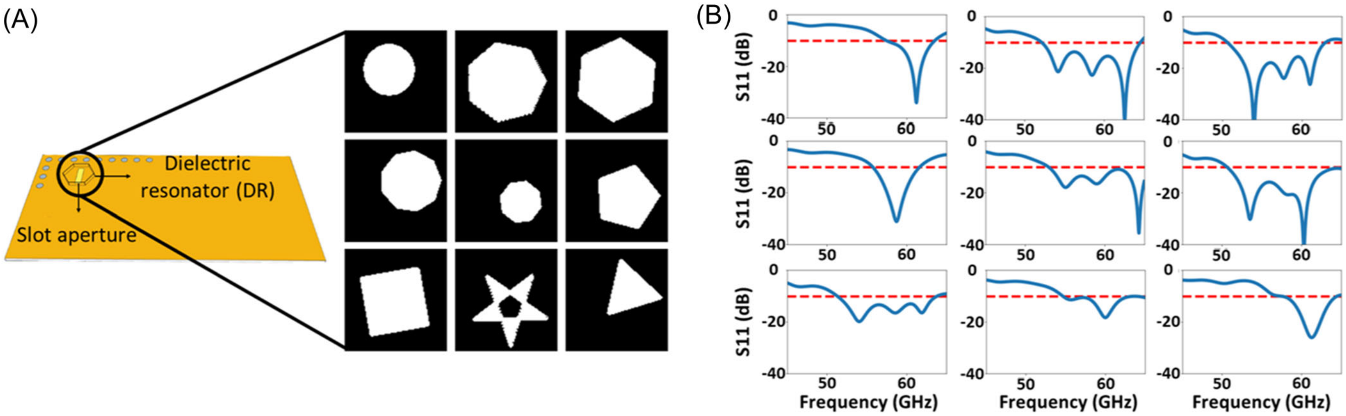

FIGURE 3 Finite element method simulation results of dielectric resonator antennas (DRAs) in the training data set. (A) Binary images of the nine representative DRA patterns. (B) Calculated S_{11} spectra of these representative DRA structures.

was used to automatically generate the FEM models based on the pixelized patterns and run the simulations for all 5040 DRAs using a high-performance computing cluster (12 CPUs, Nova cluster; Iowa State University), which took ~6 min for each simulation and 21 days in total. The final S_{11} spectra were determined by the reflection coefficient in dB. Figure 3B showcases the simulated S_{11} spectra for the selected patterns shown in Figure 3A. It can be observed that most DRAs in the training data set support one or more resonances within the 50 to 65 GHz frequency range.

3.3 | Training of the GAN model

To train the GAN model, 80% of the simulated S_{11} spectra were used as the training data and the remaining spectra were the testing ones. During the training process, the simulator (Figure 2C) was first trained using the mean-squared error (MSE) loss function, $L_S = \frac{1}{n}\sum_{i=1}^{n}|S^i - S'^i|^2$, where S is the ground truth S_{11} and S' denotes the predicted S_{11} by the simulator, and n is the dimension of S and S'. The well-trained simulator achieved an MSE of 0.6392 and 0.8637 for the training and test data sets, respectively. To train the generator along with the critic networks, we fixed the weights of the trained simulator. The loss function of the critic (L_C) and generator (L_G) was defined as follows:

$$L_C = -\frac{1}{m}\sum_{i=1}^{m}\log(C(x^i)) - \frac{1}{m}\sum_{i=1}^{m}\log(1 - C(G(S^i, z^i)))$$

$$\text{and } L_G = \frac{1}{n}\sum_{i=1}^{n}|S^i - S'^i|^2 - \lambda$$

$$\frac{1}{m}\sum_{i=1}^{m}\log(1 - C(G(S^i, z^i))),$$

where m is the batch size, x represents the ground truth pattern, S is the ground truth S_{11}, z denotes the random noise, $C(x^i)$ is the probability that the generator is rightly classifying the real image, $G(S^i, z^i)$ is the image produced by the generator, $C(G(S^i, z^i))$ is the probability that the generator misclassifies the generated image, and λ is a hyper-parameter to balance the MSE loss and cross-entropy loss. Since the minimum value of L_S was 0.8637, we searched for the best value of λ in the range of [0.1, 1] to ensure the L_1 and L_2 on the same level and get the best generator and critic performances. Here, the GAN model took 200 epochs to converge with a learning rate of 1×10^{-3} and the moving average parameter of the Adam optimizer of $\beta_1 = 0.5$ and $\beta_2 = 0.9999$.

4 | RESULTS

4.1 | Characteristics of ground truth data and loss function

The statistical results of the original data set are shown in Figure 4A,B. The S_{11} parameter was collected in the range of 50 to 65 GHz. Upon setting the band threshold as −10 dB, 2983 bands were recognized from the data set. The bands of simulated antenna designs span from 53 to 65 GHz and the minimum S_{11} values are lower than −20 dB, indicating the feasibility for practical applications. In general, the bands of higher center frequency have a wider bandwidth range. Also, the distribution of the center frequency and bandwidth emerges into four clusters implying the underlying physical principles in DRA design. The largest band found in the data set is close to 16 GHz, which is sufficient for most applications.

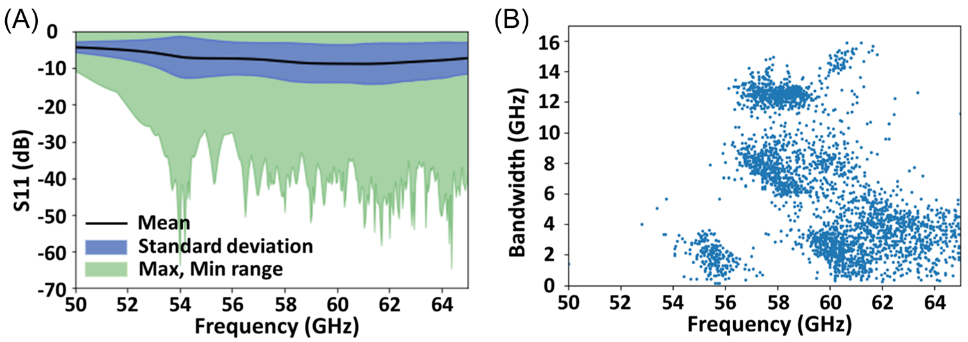

FIGURE 4 Statistical analysis of the training data set. (A) Distribution of the S_{11} spectra, and (B) −10 dB frequency bandwidth as a function of the operation frequency.

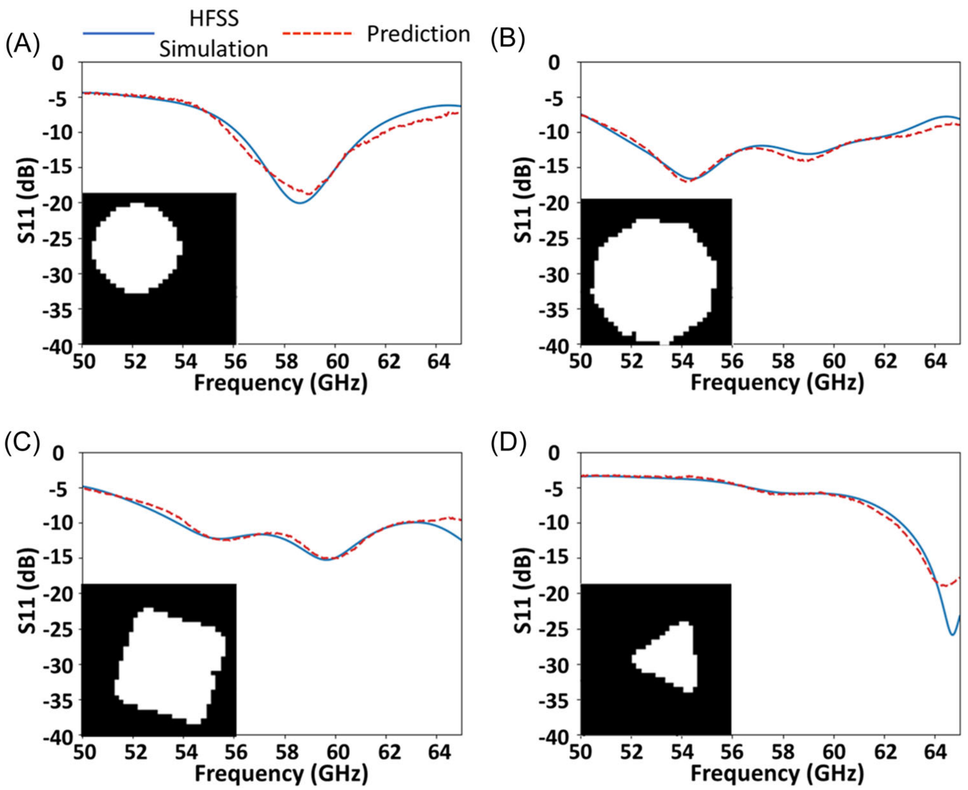

FIGURE 5 Comparision of S_{11} spectra generated by the well-trained generative adversarial network model and finite element method simulation for four different dielectric resonator antenna designs: circle (A), nonagon (B), square (C), and triangle (D).

Throughout the training process of the generator and critic networks, we observed that the loss initially converged before diverging from the minimum point. This behavior can be attributed to the inherent instability of the GAN model. To prevent divergence, an early stopping point was established during the training process. The top five model candidates were manually examined to verify the accuracy of the generated antenna patterns, and one of these five models was selected for further evaluation experiments.

4.2 | Prediction of DRA's S_{11}

The trained GAN model was used to replace the full-wave FEM model for calculating the S_{11} spectra of new DRA designs. The HMSIW substrate and the thickness of the dielectric resonators remained the same as described in Section 2.2. Four patterns, which were not included in the training data set, were chosen to evaluate the trained GAN model's S_{11} prediction performance. The 2D antenna designs were pixelized into the 32×32 binary arrays and then input into the simulator of the GAN

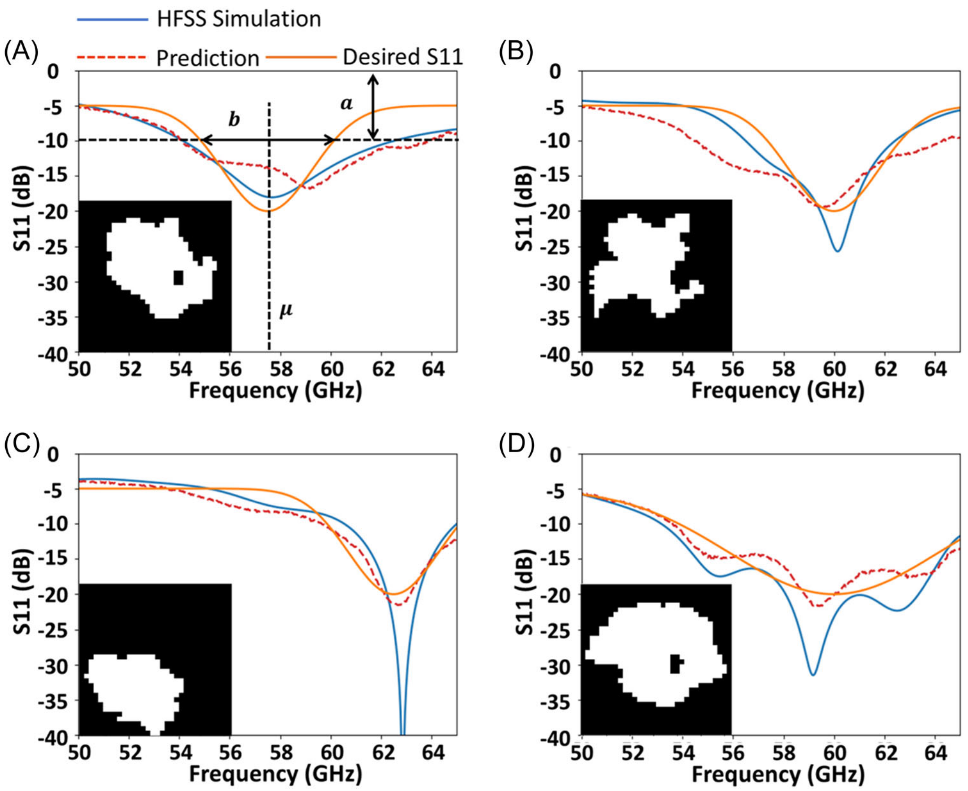

FIGURE 6 Dielectric resonator antenna patterns generated by the generator network. The comparison between the desired Gaussian-like S_{11} spectrum with ($a = 10$ dB, $b = 6$ GHz, $\mu = 57.5$ GHz) for (A), ($a = 10$ dB, $b = 6$ GHz, $\mu = 60$ GHz) for (B), ($a = 10$ dB, $b = 6$ GHz, $\mu = 62.5$ GHz) for (C), ($a = 10$ dB, $b = 12$ GHz, $\mu = 60$ GHz) for (D), and the corresponding GAN-generated DRA patterns.

model. The predicted S_{11} spectra were output from the deep learning model correspondingly. The patterns, as shown in the insets of Figure 5, were the inputs of the GAN model. Figure 5 compares the S_{11} spectra calculated using the GAN model and the FEM simulation directly. It can be seen that the GAN predicted S_{11} spectra agree well with the FEM simulation results. For these four examples, the frequency-averaged GAN model calculation error is less than 0.42 dB within the 50–65 GHz range. Apart from some extreme resonance cases, the simulator can capture the main resonance features in S_{11} spectra. At resonance frequencies with more than 20 dB reflection, the GAN prediction results exhibited an error of 2.2 dB, which is acceptable for the antenna design with 10 dB as the desired reflection threshold.

4.3 | Intelligent design of DRA structures

The GAN model can also be implemented to generate new DRA patterns based on a given S_{11} spectra. The cGAN model was trained to generate realistic antenna patterns on the condition of desired S_{11} spectra to minimize the loss between given S_{11} spectra and predicted S_{11} spectra from the Simulator. The deep learning model was converged to learn the intrinsic principle of antenna design. To illustrate the capability of GAN inverse design function, four desired S_{11} spectra were given to the trained GAN model. As shown in Figure 6, both S_{11} spectra have the Gaussian shape with the band threshold, bandwidth, and center frequency of a, b, and μ, respectively. For the spectrum in Figure 6A–D, we set the band threshold a as 10 dB for (A–D), the bandwidth b as 6 GHz for (A–D), the center frequency μ as 57.5 GHz for (A), 60.0 GHz for (B), 62.5 GHz for (C), and 60.0 GHz for (D), respectively. The GAN-generated patterns are shown in the insets of Figure 6. These shapes from the generator were not presented in the original 5040-sample data set. The generated designs seem a combination of one or two shapes in the ground truth data set but with some differences on the edge. For example, the output antenna shape in (A) is a combination of square and triangle, while the other shape in (B) is a part of star. Meanwhile, it is observed that the S_{11} parameter of generated antenna designs matches well with the main feature of desired S_{11} response, especially the bandwidth and center frequency coefficients.

5 | CONCLUSION

This paper introduces a GAN-enabled method for automating the design of mmWave DRAs. We proposed a novel GAN structure that was trained using paired antenna shapes and their corresponding S_{11} spectra. The final model has been verified for the performance of forward prediction and inverse design using the existing data set. Moreover, we observed that the model has learned the fundamental principles of DRA design and generated novel antenna shapes based on the desired S_{11} characteristics. This proposed method has the potential to be extended for the design of other types of antennas. This study recognizes the constraints arising from the limited size of the data set used in training our model. Currently, the model is designed to consider only the S_{11} parameters. To develop a more comprehensive machine learning model, our future work will involve expanding the data set and incorporating additional parameters, including radiation pattern and efficiency. Additionally, we are considering the application of alternative neural network architectures, such as physics-informed neural networks, to enhance convergence efficiency.

ACKNOWLEDGMENTS

This research was supported by the National Science Foundation under grant ECCS 16-53673. Any opinions, findings, and conclusions or recommendations expressed in this material are those of the author(s) and do not necessarily reflect the views of the National Science Foundation. Open access funding provided by the Iowa State University Library.

DATA AVAILABILITY STATEMENT

The data that support the findings of this study are openly available in AntennaGAN at https://github.com/mingdianliu/AntennaGAN.

REFERENCES

1. Keyrouz S, Caratelli D. Dielectric resonator antennas: basic concepts, design guidelines, and recent developments at millimeter-wave frequencies. *Int J Antennas Propag*. 2016;2016:6075680. doi:10.1155/2016/6075680
2. Mukherjee B, Patel P, Mukherjee J. A review of the recent advances in dielectric resonator antennas. *J Electromagn Waves Appl*. 2020;34(9):1095-1158.
3. Rashidian A, Tayfeh Aligodarz M, Shafai L, Klymyshyn DM. On the matching of microstrip-fed dielectric resonator antennas. *IEEE Trans Antennas Propag*. 2013;61(10):5291-5296.
4. Mukherjee B, Patel P, Mukherjee J. A novel cup-shaped inverted hemispherical dielectric resonator antenna for wide-band applications. *IEEE Antennas Wirel Propag Lett*. 2013;12:1240-1243.
5. Surendra L, Khan H. Design and analysis of cylindrical dielectric resonator antenna for 5G application. *Int J Eng Adv Technol*. 2020;10(2):116-119.
6. Ali I, Jamaluddin MH, Gaya A, Rahim HA. A dielectric resonator antenna with enhanced gain and bandwidth for 5G applications. *Sensors*. 2020;20(3):675.
7. Yao HM, Jiang L, Sha WEI. Enhanced deep learning approach based on the deep convolutional encoder–decoder architecture for electromagnetic inverse scattering problems. *IEEE Antennas Wirel Propag Lett*. 2020;19(7):1211-1215.
8. Yao HM, Sha WEI, Jiang L. Two-step enhanced deep learning approach for electromagnetic inverse scattering problems. *IEEE Antennas Wirel Propag Lett*. 2019;18(11):2254-2258.
9. Key C, Notaros B. Predicting macro basis functions for method of moments scattering problems using deep neural networks. *IEEE Antennas Wirel Propag Lett*. 2021;20(7):1200-1204.
10. Jacobs JP. Accurate modeling by convolutional neural-network regression of resonant frequencies of dual-band pixelated microstrip antenna. *IEEE Antennas Wirel Propag Lett*. 2021;20(12):2417-2421.
11. Goodfellow I, Pouget-Abadie J, Mirza M, et al. Generative adversarial networks. *Commun ACM*. 2020;63(11):139-144.
12. Wang HP, Li YB, Li H, et al. Deep learning designs of anisotropic metasurfaces in ultrawideband based on generative adversarial networks. *Adv Intell Syst*. 2020;2(9):2000068.
13. Liu Z, Zhu D, Rodrigues SP, Lee KT, Cai W. Generative model for the inverse design of metasurfaces. *Nano Lett*. 2018;18(10):6570-6576.
14. Naseri P, Hum SV. A generative machine learning-based approach for inverse design of multilayer metasurfaces. *IEEE Trans Antennas Propag*. 2021;69(9):5725-5739.
15. Liu M, Zhang H, Lu M, Song J. Generative adversarial network-based design of dielectric resonator antenna for mmWave 5G applications. In: *2021 IEEE International Symposium on Antennas and Propagation and USNC-URSI Radio Science Meeting, APS/URSI 2021*, Singapore, Singapore. Institute of Electrical and Electronics Engineers Inc.; 2021:1877-1878. doi:10.1109/APS/URSI47566.2021.9704678
16. Qinghua Lai L, Fumeaux C, Wei Hong H, Vahldieck R. 60 GHz aperture-coupled dielectric resonator antennas fed by a half-mode substrate integrated waveguide. *IEEE Trans Antennas Propag*. 2010;58(6):1856-1864.
17. Mirza M, Osindero S. Conditional generative adversarial nets. *arXiv*. Preprint posted online November 6, 2014. http://arxiv.org/abs/1411.1784
18. Odena A, Olah C, Shlens J. Conditional image synthesis with auxiliary classifier GANs. In *International conference on machine learning*. PMLR; 2017:2642-2651. https://arxiv.org/abs/1610.09585
19. Chen X, Duan Y, Houthooft R, Schulman J, Sutskever I, Abbeel P. InfoGAN: interpretable representation learning by information maximizing generative adversarial nets. *Advances in Neural Information Processing Systems*. 2016;29. https://arxiv.org/abs/1606.03657
20. Krizhevsky A, Sutskever I, Hinton GE. ImageNet classification with deep convolutional neural networks. *Commun ACM*. 2017;60:84-90.
21. Ioffe S, Szegedy C. Batch normalization: accelerating deep network training by reducing internal covariate shift. In *International conference on machine learning*. PMLR; 2015:448-456. doi:10.48550/arXiv.1502.03167

22. He K, Zhang X, Ren S, Sun J. Deep residual learning for image recognition. In: *Proceedings of the IEEE Conference on Computer Vision and Pattern Recognition (CVPR)*. IEEE; 2016:770-778. http://image-net.org/challenges/LSVRC/2015/
23. Korchi AEl, Ghanou Y. 2D geometric shapes dataset—for machine learning and pattern recognition. *Data Brief*. 2020;32:106090.

How to cite this article: Liu M, Zhang H, Song J, Lu M. Using generative model for intelligent design of dielectric resonator antennas. *Microw Opt Technol Lett*. 2024;66:e34013. doi:10.1002/mop.34013